Dalton Transactions

Formation of $PbCl_2$-type AHF (A = Ca, Sr, Ba) with Partial Anion Order at High Pressure

Journal:	*Dalton Transactions*
Manuscript ID	DT-ART-03-2021-001054.R1
Article Type:	Paper
Date Submitted by the Author:	03-May-2021

Complete List of Authors:	Tsuchiya, Yumi; Kyoto University, Department of Energy and Hydrocarbon Chemistry Wei, Zefeng; Kyoto University, Department of Energy and Hydrocarbon Chemistry Broux, Thibault; Kyoto University, Department of Energy and Hydrocarbon Chemistry Tassel, Cédric ; Kyoto University, Department of Energy and Hydrocarbon Chemistry Ubukata, Hiroki; Kyoto University, Department of Energy and Hydrocarbon Chemistry Kitagawa, Yuuki; Kyoto University, Graduate School of Human and Environmental Studies Ueda, Jumpei; Kyoto University, Tanabe, Setsuhisa; kyoto university, Grad School of HES; Kyoto University Kageyama, Hiroshi; Kyoto University, Department of Energy and Hydrocarbon Chemistry

ARTICLE

Formation of $PbCl_2$-type AHF (A = Ca, Sr, Ba) with Partial Anion Order at High Pressure

NDReceived 00th January 20xx,
Accepted 00th January 20xx

DOI: 10.1039/x0xx00000x

Yumi Tsuchiya,‡[a] Zefeng Wei,‡[a] Thibault Broux,[a] Cédric Tassel,[a] Hiroki Ubukata,[a] Yuuki Kitagawa,[b] Jumpei Ueda,[b] Setsuhisa Tanabe,[b] and Hiroshi Kageyama*[a]

The high-pressure structures of alkaline earth metal hydride-fluorides AHF (A = Ca, Sr, Ba) were investigated up to 8 GPa. While AHF adopts the fluorite-type structure ($Fm\bar{3}m$) at ambient pressure without anion order, the $PbCl_2$-type (cotunnite-type) structure (*Pnma*) is formed by pressurization, with a declining trend of critical pressure as the ionic radius of A^{2+} cation increases. In contrast to $PbCl_2$-type LaHO and LaOF whose anions are fully ordered, H^-/F^- anions in the high-pressure polymorph of SrHF and BaHF are partially ordered, with a preferential occupation of H^- at the square-pyramidal site (vs. tetrahedral site). First-principles calculations partially support the preferential anion occupation and suggest occupation switching at higher pressure. These results provide a strategy for controlling anion ordering and local structure in mixed-anion compounds.

Introduction

Hydride (H^-) anion has unique features that are not found in other anions such as O^{2-}, N^{3-} and F^-.[1] For example, the possession of two electrons only in 1s orbitals means the lack of π symmetry, which enables perovskite $SrVO_2H$ and its layered analogues to have low-dimensional Mott insulating states owing to the non-bonding nature between V t_{2g} and H 1*s* orbitals.[2–4] Furthermore, the lability of hydride anions in perovskite oxyhydride $BaTi(O,H)_3$ makes it a useful precursor for the synthesis of other mixed-anion compounds (e.g, $BaTi(O,N)_3$ and $BaTi(O,F)_3$[5,6]) and also a promising catalyst or support for ammonia synthesis and CO_2 reduction.[7,8]

More recently, the hydride anions are shown to be highly compressible, twice as compressible as oxide anions, by high-pressure X-ray diffraction study of $SrVO_2H$.[2] This feature is also responsible for anion order-disorder transition in fluorite-type LnHO (Ln = lanthanide).[9] Further study on LnHO revealed that hydride diffusion is enabled by anion ordering with the increase of Ln^{3+} radius which expands the bottleneck for the H^- conduction pathway.[10] Moreover, when the external pressure is applied to anion-ordered fluorite-type LaHO (*P*4/*nmm*),[9] two polymorphs appear: $PbCl_2$-type γ-LaHO (*Pnma*) at 3 GPa and anti-Fe_2P-type δ-LaHO ($P\bar{6}2m$) at 5 GPa.[11] The 3 GPa phase consists of HLa_5 square pyramids and OLa_4 tetrahedra, whereas in the 5 GPa phase, the coordination geometries are swapped, with OLa_5 square pyramids and HLa_4 tetrahedra. This coordination reversal is unprecedented since the coordination number around hydride decreases from 5 to 4 at a higher pressure. However, given the distinct compressibility between H^- and O^{2-} leading to different responses in size upon external pressure, this phenomenon can be understood within the framework of Pauling's first rule.

The effect of hydride size flexibility may also appear when combined with anions other than oxide anions. In fact, the bulk modulus of rock-salt-type NaF (53.8 GPa)[12] is smaller than that of isostructural CaO (111 GPa),[13] but still much larger than that of NaH (19.4 GPa).[14] It is thus expected that the higher compressibility of hydride anions (vs. fluoride anions) in hydride-fluoride compounds would allow novel crystal and local structures, as observed in LaHO.[9-11] Based on these considerations, in the present study we targeted the alkaline earth metal hydride-fluorides AHF (A = Ca, Sr, Ba), whose anions are fully disordered at ambient pressure.[15,16] We carried out the high-pressure synthesis and structural characterization of AHF up to 8 GPa. Experimental results of structural transitions to the $PbCl_2$-type structure, anion order-disorder behaviour, and A-site dependence are discussed, including first-principles calculations.

Results and discussion

Pressure-induced phase transition

[a] *Department of Energy and Hydrocarbon Chemistry, Graduate of School of Engineering, Kyoto University, Nishikyo-ku, Kyoto 615-8510, Japan. Email: kage@scl.kyoto-u.ac.jp*
[b] *Graduate School of Human and Environmental Studies, Kyoto University, Sakyo-ku, Kyoto 606-8501, Japan.*

†Electronic Supplementary Information (ESI) available: [details of any supplementary information available should be included here]. See DOI: 10.1039/x0xx00000x

‡These authors contributed equally to the publication.

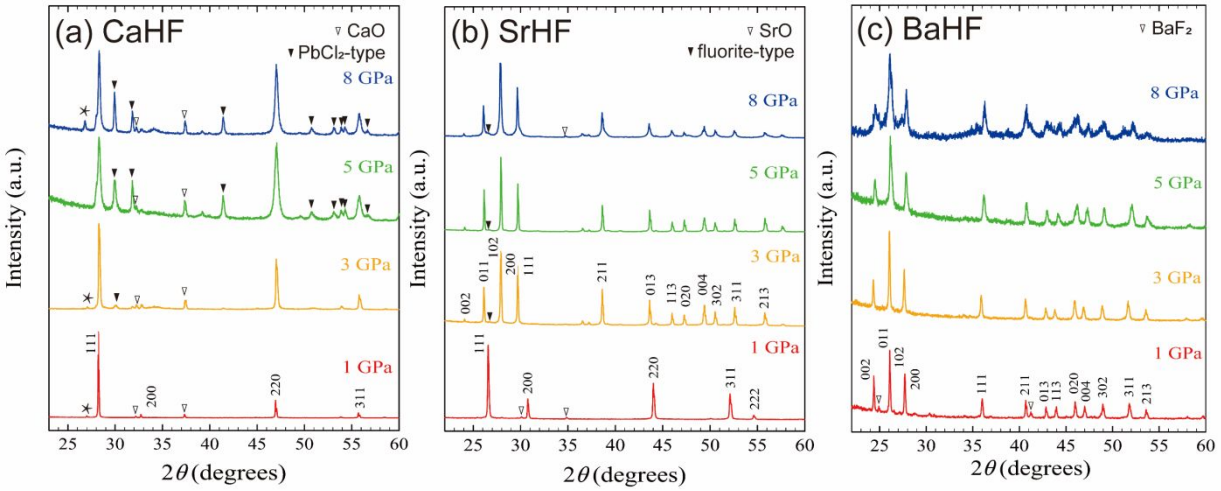

Fig. 1 XRD patterns of (a) CaHF, (b) SrHF, (c) BaHF synthesized under 1, 3, 5, and 8 GPa. For CaHF, the molar fraction of the $PbCl_2$-type structure is 6%, 24% and 25% at 3, 5, and 8 GPa, respectively. Unknown peaks are indexed by asterisks.

AHF (A = Ca, Sr, Ba) prepared at ambient conditions adopt the cubic fluorite-type structure ($Fm\bar{3}m$) without any anion ordering.[15,16] Figure 1b displays laboratory X-ray diffraction (XRD) patterns of SrHF synthesized at 1, 3, 5, and 8 GPa. At 1 GPa (SrHF-1GPa), the diffraction pattern resembles that of the ambient-pressure phase.[17] A small amount of SrO (2.5%) was found as an impurity phase. Compared with fluorite-type SrF_2 at ambient pressure (a = 5.80 Å), SrHF has a somewhat larger lattice parameter of a = 5.8274(1) Å. No superstructure reflection associated with anion order was detected. When SrHF was synthesized at 3 GPa, however, there appears a completely different pattern, which can be indexed using an orthorhombic cell with a = 6.3673(2) Å, b = 3.8403(1) Å, and c = 7.3893(3) Å. These values are close to those of the pressure-induced phase of AF_2 (A = Ca, Sr, Ba) having the $PbCl_2$-type (*Pnma*) structure (e.g., for SrF_2, a = 6.154(5) Å, b = 3.645(1) Å and c = 7.312(3) Å at 15.2 GPa).[18] Similar XRD patterns are obtained for SrHF samples prepared at 5 GPa and 8 GPa (Figure 1b). A small amount of SrO and fluorite-type SrHF were found as the impurity phases. The presence of the small amount of fluorite-type SrHF might indicate retransformation from the high-pressure phase during decompression process.[19]

The XRD profile for BaHF samples synthesized under pressure (Figure 1c) indicates that the structural phase transition to the $PbCl_2$-type structure has already occurred at 1 GPa. A small amount of BaF_2 impurity (7.0%) was found. Reflecting the difference in ionic radii of A^{2+} cations, the orthorhombic cell parameters for BaHF (a = 6.8381(2) Å, b = 4.1225(1) Å, and c = 7.8938(2) Å at 1 GPa) are greater than that for SrHF.

An opposite trend is seen for CaHF with a smaller cationic radius. As shown in Figure 1a, the XRD pattern of the 3 GPa sample contains a $PbCl_2$-type phase, but with a small molar fraction of 6%, along with a CaO impurity (5.2%). The phase transition to the $PbCl_2$-type structure is also incomplete at higher pressure; the volume fraction of the $PbCl_2$-type phase is 25% even at 8 GPa. These observations suggest that a smaller alkaline earth metal cation can extend the fluorite-type structure to a higher pressure range. The pressure-dependent AHF structural transition is summarized as a function of the Shannon ionic radius of alkaline earth cations (Figure 2).

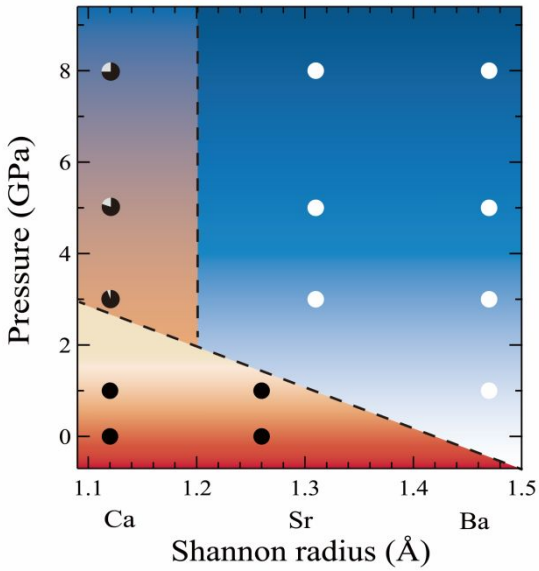

Fig. 2 A phase diagram for AHF (A = Ca, Sr, Ba) synthesized under pressure of 1, 3, 5 and 8 GPa, plotted as a function of Shannon radius of A^{2+} cations. Filled and open circles denote, respectively, fluorite-type structure (*Fm*-3*m*) and $PbCl_2$-type structure (*Pnma*). For A = Sr and Ba, the Shannon radius of 8- and 9-coordination are employed for the fluorite- and $PbCl_2$-type structures, respectively.[26] Data at ambient pressure are taken from references.[15,16]

The AF_2 analogues also undergo a structural phase transition from the fluorite-type structure to the $PbCl_2$-type structure. As in the case of AHF, the critical pressure of AF_2 decreases as the size of A cation increases (9.5 GPa for Ca, 5.0 GPa for Sr, and 3.8 GPa for Ba).[18, 20–21] For a given A cation, the critical pressure of AHF is lower than that of AF_2, which is naturally understood since AH_2 crystallizes in the $PbCl_2$-type structure at ambient pressure (for the critical pressure, AH_2 < AHF < AF_2). Likewise, both AH_2 and AF_2 undergo a phase transition from $PbCl_2$-type structure to Ni_2In-type structure at 15, 7.8, and 1.6 GPa for AH_2 (A = Ca, Sr, Ba) [22–24] and 63, 28, and 15 GPa for AF_2 (A = Ca, Sr, Ba).[20,25] In our present study, this Ni_2In-type phase is not observed even with BaHF up to 8 GPa, though we speculate that the Ni_2In-type structure may appear at higher pressure.

Structural refinement

Synchrotron powder X-ray diffraction (SXRD) and powder neutron diffraction (PND) data at room temperature for SrHF-1 GPa do not exhibit any superstructure reflections (Figures S1, S2 and Tables S1, S2), in agreement with the previous study on anion-disordered SrHF at ambient pressure.[16] Rietveld refinement analysis was carried out using the anion-disordered fluorite-type structure ($Fm\bar{3}m$), with Sr at the 4*a* site, and H/F at the 8*c* site. SrH_2 (5.9%) and SrO (5.0%) were included as the secondary and ternary phases. The fitting from PND data successfully converged and gave reasonable reliability parameters of R_p = 5.71% and R_{wp} = 6.97%. The similar occupancy factors of *g*(H) = 0.4892(1) and *g*(F) = 0.5107(1) means that H^- and F^- anions are fully disordered at the 8*c* site (Figure 3).

For SrHF-3GPa, we constructed a model using the $PbCl_2$-type structure (*Pnma*). This structure has the Wyckoff 4*c* site for the Sr^{2+} cation, while there are two different anionic (4*c*) positions, a tetrahedral (X1) site and a square-pyramidal (X2) site, as shown in Figure 4b. In our previous study on LaHO with

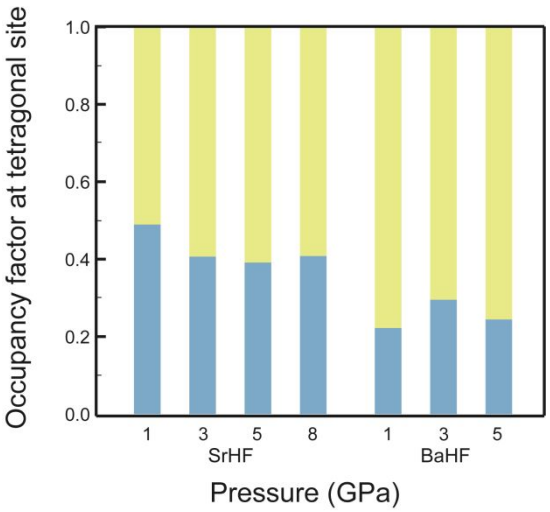

Fig. 3 The occupancy factors of anion at the tetragonal site for SrHF and BaHF at different synthesized pressures, taken from the structural analysis of PND data (SrHF-1 GPa, SrHF-3 GPa, and BaHF-1 GPa) and SXRD data (SrHF-5 GPa, SrHF-8 GPa, BaHF-3 GPa, BaHF-5GPa). Blue and yellow bars represent H and F, respectively.

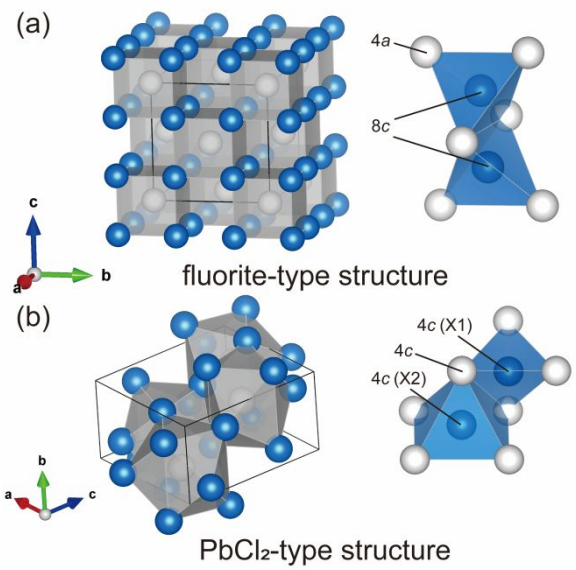

Fig. 4 (a) Fluorite-type structure (*Fm*-3*m*) and (b) $PbCl_2$-type structure (*Pnma*). The right side of each panel represents a coordination environment around the anion center: (a) the tetrahedral 8*c* site and (b) the tetrahedral 4*c* (X1) and the square-pyramidal 4*c* (X2) site. The white and blue balls represent A cations (Ca, Sr, Ba) and X anions (H, F), respectively. Solid lines represent the unit cell.

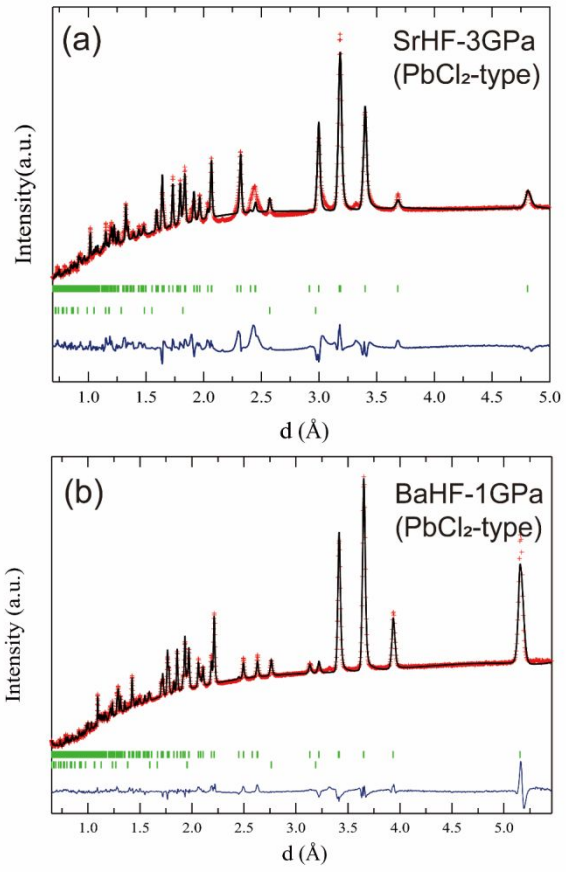

Fig. 5 Rietveld refinements of PND data for (a) SrHF at 3 GPa, and (b) BaHF at 1 GPa. The red, black, and blue lines represent the observed, calculated, and residual curves, respectively. Green ticks indicate the peak positions. The lower green ticks in (a) are SrO (1.9%) and (b) are BaO (2.8%) as impurities.

the $PbCl_2$-type structure at 3 GPa,[11] H^- anions exclusively occupy the square-pyramidal site while O^{2-} at the tetrahedral site. Since the ionic radii for O^{2-} and F^- are close to each other (1.35 Å and 1.285 Å),[26] we assumed an anion ordering with H^- at the square-pyramidal site (as in LaHO[11]) and F^- at the tetrahedral site, which resulted in a rather poor agreement with R_p = 9.25% and R_{wp} = 13.1% (Figure S3). However, a significant improvement was achieved when the anti-site disorder was taken into consideration, yielding R_p = 3.71% and R_{wp} =5.62% (Figure 5a). Here, H^- and F^- anions were constraint to be 'stoichiometric' (i.e., SrHF). Importantly, H^- and F^- anions are not fully disordered, as opposed to the ambient-pressure fluorite-type phase (SrHF-1 GPa) whose anions are fully disordered (Figure 3). The square-pyramidal (X2) site is preferred for H^-, with an occupancy factor *g*(H2) of 0.5936(2) (Table 1). The Rietveld refinements of SXRD data for SrHF synthesized at 5 and 8 GPa also converged with the partial anion-ordered structure with preferential hydride occupation at the 5-coordinate site, with the similar occupancy factors of *g*(H2) = 0.609(2) and *g*(H2) = 0.592(2), respectively (Figures S5, S6, and Tables S4, S5). For BaHF, the structural analysis of PND data at 1 GPa again led to the preferential occupation (Figure 5b, Table 1). However, as compared with SrHF, the hydride anion in BaHF has a higher preference for the square-pyramidal site with *g*(H2) = 0.7781(3). In other words, the tetragonal site is preferred for F^-, as shown in Figure 3.

Table 1 Structural parameters of (upper) SrHF synthesized at 3 GPa and (lower) BaHF synthesized at 1 GPa determined from Rietveld refinement on PND data. For SrHF (*Pnma*), a = 6.36501(5) Å, b = 3.83913(3) Å, c = 7.38149(6) Å, R_p = 4.21% and R_{wp} = 6.14%, and for BaHF (*Pnma*), a = 6.84423(4) Å, b = 4.13075(2) Å, c = 7.88663(5) Å, R_p = 1.84% and R_{wp} = 2.44%. (Wyckoff position for all atoms is 4*c*)

atom	*x*	*y*	*z*	B_{iso} (Å^2)	*g*
Sr	0.23372(4)	0.25	0.11279(3)	0.634(5)	1*
H1	0.35889(10)	0.25	0.41912(12)	1*	= 1 – *g*(H2)
H2	0.984(3)	0.25	0.641(3)	1*	0.5936(2)
F1	= *x*(H1)	0.25	= *z*(H1)	1*	= *g*(H2)
F2	= *x*(H2)	0.25	= *x*(H2)	1*	= 1 – *g*(H2)

atom	*x*	*y*	*z*	B_{iso} (Å^2)	*g*
Ba	0.24198(6)	0.25	0.11191(3)	0.964(8)	1*
H1	0.36059(5)	0.25	0.42866(5)	1*	= 1 – *g*(H2)
H2	0.97713(14)	0.25	0.68330(9)	1*	0.7781(3)
F1	= *x*(H1)	0.25	= *z*(H1)	1*	= *g*(H2)
F2	= *x*(H2)	0.25	= *z*(H2)	1*	= 1 – *g*(H2)

*fixed to be 1.

The Origin of Partial Anion Order

The present results, together with the previous study, have revealed that both LaHO and AHF with the fluorite-type structure undergo the pressure-induced phase transition to the $PbCl_2$-type structure. However, the anion order-disorder behaviour is quite different. The anions in $PbCl_2$-type LaHO (also for the anti-Fe_2P-type LaHO at higher pressure) are fully ordered. For AHF, H^- and F^- are fully disordered in the ambient pressure fluorite-type structure, while in the $PbCl_2$-type structure, partial anion order is present at the tetrahedral site (four-coordinate) and the square-pyramidal (five-coordinate) site (Figure 3). The degree of anion order, 2 × *g*(H2) – 1, where *g*(H2) is the occupancy of H at the square-pyramidal site, are 0.187 and 0.556 for SrHF (3 GPa) and BaHF (1 GPa), respectively, indicating that the anion order is more prominent for the latter. Given the anion disorder of AHF for the fluorite-type structure having only four coordination number around anions, the different coordination numbers (4 and 5) in the $PbCl_2$-type structure could play a key role in generating the partial anion ordering, though anions in fluorite-type LnHO with larger lanthanide cations (Ln = La, Ce, Pr, Nd) is fully anion-ordered.[9] Anions in $PbCl_2$-type LnOF (Ln = Nd, Sm, Er) is, like LaHO, fully anion-ordered with OLa_4 tetrahedra and FLa_5 square pyramids.[27] Thus, it may be claimed that the inequivalence in anion valence (H^-/O^{2-} and F^-/O^{2-} vs. F^-/H^-) is essential for the complete anion order as found in double perovskite $A_2BB'O_6$.[28] Bond valence sums (BVS) calculations for the hydride anion are difficult since its ionic radius greatly changes depending on the surrounding environment.[2] Accordingly, the BVS for fluoride anion was calculated using the PND results of SrHF-3GPa and BaHF-1GPa. For SrHF, we obtained –1.32 for the tetrahedral site and –0.83 for the square-pyramidal site. Similar values are obtained for BaHF with –1.24 and –0.70 for the tetrahedral and square-pyramidal site. It means that the square-pyramidal (five-coordinate) site is underbonded and the tetrahedral site (four-coordinate) is overbonded for F^-. Therefore, it is possible that the suppression of the fluorine underbonding state at the five-coordinate site may lead to the preferential occupation of the four-coordinate site. The five-coordinate site with the majority of H^- might be stabilized by expanding the size of hydride anions.

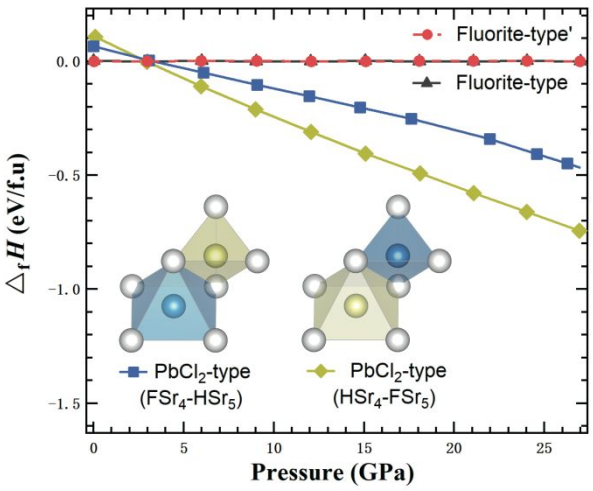

Fig. 6 Calculated formation enthalpies as a function of pressure of $PbCl_2$-type SrHF (relative to fluorite-type SrHF). The two models of anion-ordered fluorite-type SrHF were built from anion-ordered LaHO (*P4/nmm*) with reverse anionic site occupancy, in order to represent anion-disorder fluorite-type SrHF. The local coordination geometries around the anion center are shown, where the white, blue and yellow spheres represent Sr, H and F, respectively.

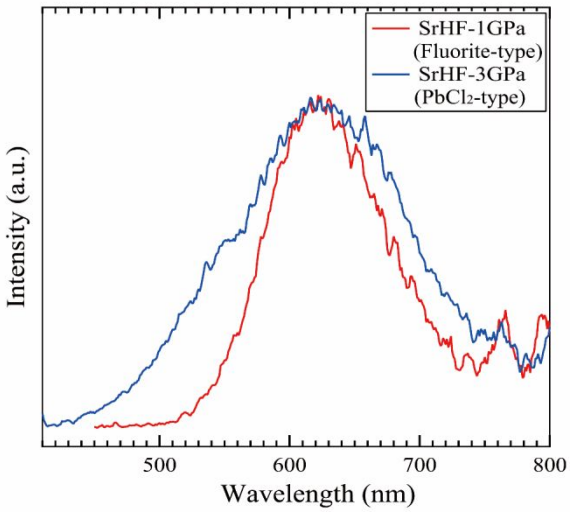

Fig. 7 Photoluminescence spectra of SrHF: Eu^{2+} with fluorite-type (1 GPa) and $PbCl_2$-type (3 GPa) structures collected at room temperature.

First-principles calculations were conducted in order to mainly investigate the anionic site occupancy of $PbCl_2$-type SrHF under different pressures, where for simplicity, we only considered two fully anion-ordered models with reverse anionic site occupancy (Figure 6). For $PbCl_2$-type SrHF, at low pressure, the FSr_4-HSr_5 model shows lower formation enthalpy than that of the HSr_4-FSr_5 model, but the HSr_4-FSr_5 model is more stable at higher pressure. It implies that the anion coordination reversal of H^- and F^- could be induced by external pressure, which means the reduction in coordination number of H^- by pressurization ($HSr_5 \rightarrow HSr_4$). Such phenomenon is only experimentally observed at LaHO ($PbCl_2$-type OLa_4-HLa_5 at 3 GPa $\rightarrow$ anti-Fe_2P-type HLa_4-OLa_5 at 5GPa) originating from high compressibility of H^-.[11] However, this coordination reversal in $PbCl_2$-type SrHF with partial anion order is not seen in the pressure range examined, which might be due to the fact that temperature was not taken into account in the calculation or that anion rearrangement occurs during the decompression process after synthesis. The latter scenario may be supported by almost the same anionic occupancy factors for $PbCl_2$-type SrHF synthesized at 3, 5, 8 GPa (Table 2). Theoretically, a pressure-induced reversal of anion coordination is seen in anti-Fe_2P-type ($HSr_5 \rightarrow HSr_4$) and Ni_2In-type SrHF ($HSr_6 \rightarrow HSr_5$) (Figure S15). Therefore, not limited to this system, it is expected that pressure-induced coordination transformation is generically observed in mixed-anion compounds containing hydride.

Photoluminescence Properties

Fluorite-type compounds function as a host of phosphor, and hydride incorporation can shift the emission wavelength to a longer wavelength due to nephelauxetic effect, as shown by EuHF, EuHCl, GdHO: Tb, $NaMg(H,F)_3$: Eu.[29–32] Since fluorescent properties are largely affected by coordination environment around cations, one can expect that the change in coordination number by the structural phase transition will influence fluorescent properties. We prepared SrHF: Eu^{2+} (1%) samples with fluorite-type (1 GPa) and $PbCl_2$-type (3 GPa) structures and collected Photoluminescence (PL) spectra. Figure 7 shows the respective PL spectra measured at room temperature using excitation wavelengths of 390 nm for the fluorite-type and 340 nm for the $PbCl_2$-type samples. Given the emission wavelengths of SrF_2: Eu^{2+} (416 nm) and SrH_2: Eu^{2+} (728 nm),[34,35] the peak centered at 624 nm, ascribed to the $4f^65d^1 \rightarrow 4f^7$ transition of Eu^{2+}, for both fluorite-type and $PbCl_2$-type SrHF: Eu^{2+} is reasonable. The slight change of emission wavelengths for the cubic to orthorhombic phase transition also occurs in SrF_2: Eu^{2+} in the pressure range of 0-8 GPa.[36,37] However, the peak of $PbCl_2$-type compound is broader than that of fluorite-type compound,[37] which might originate from a larger offset of configurational coordinate caused by longer bond lengths between Eu^{2+} and ligands in $PbCl_2$-type SrHF (average bond length: 2.60 Å) than that in fluorite-type SrHF (2.52 Å). In addition, the highly symmetrical cuboid-like local coordination environment in fluorite-type SrHF: Eu^{2+} (SrH_4F_4) may also contribute to narrower bandwidth.[38]

Conclusions

To sum up, we have investigated the structural evolution of AHF (A = Ca, Sr, Ba) under high pressure and found a phase transition from the anion-disordered fluorite-type structure to the partial anion-ordered $PbCl_2$-type structure. The partial order of AHF in the $PbCl_2$-type structure, as opposed to the complete disorder in the ambient-pressure fluorite-type AHF, is related to the presence of different coordination environments around anions. The preferential occupancy of H^- at the square-pyramidal site (vs. tetrahedral site) in $PbCl_2$-type AHF is similar to the isostructural LaHO and LaOF, but the

partial order in AHF could be related to the fact that both anions are monovalent. Theoretical calculations also support the preferential occupancy of H^- at the square-pyramidal (HSr_5) site at low pressure, with a potential coordination switching at higher pressure. This study suggests a possible control of the structure and anionic occupancy in hydride-based mixed-anion compounds by varying pressure, which may lead to the development of novel crystal and local structures with tuned occupancies of anions.

Materials and Methods

Polycrystalline AHF samples (A = Ca, Sr, Ba) were synthesized via high-pressure, high-temperature solid-state reactions using stoichiometric amounts of hydrides and fluorides. For CaHF, starting materials, CaH_2 (ALDRICH, > 97.0%) and CaF_2 (ALDRICH, 99.99%), were intimately mixed and pelletized in a nitrogen-filled glovebox. The pellet was inserted in a BN sleeve and capped with two BN caps. The assembled sleeve was placed in a graphite tube heater and enclosed in a pyrophylite cell. After elevating a pressure to 1, 3, 5, or 8 GPa using a cubic anvil press, the temperature was raised to 600 °C in 10 minutes, held for 1 hour, and then cooled to room temperature in 5 minutes, followed by pressure release. Likewise, SrHF and BaHF samples were synthesized, but with a higher reaction temperature of 900 °C. Starting reagents of SrH_2 (Mitsuwa chemicals, 99.5%), BaH_2 (Mitsuwa chemicals, 99.5%), SrF_2 (Wako, 99.5%) and BaF_2 (ALDRICH, 99.99%) were used as received.

The obtained samples were characterized by powder X-ray diffraction (XRD), using a D8 ADVANCE diffractometer (Bruker AXS) with Cu-K_α radiation. Powder synchrotron XRD experiments (SXRD) were performed at room temperature on a Debye-Scherrer camera at the BL02B2 and BL32B2 beamline at SPring-8. Since the AHF samples are slightly air sensitive, the samples were sealed in Pyrex capillaries under N_2 atmosphere. The capillary was rotated during the measurements to reduce the effect of preferred orientation of crystals. Rietveld refinement was performed using the Fullprof package.[39] Neutron diffraction measurements for SrHF and BaHF were performed at room temperature using a time-of-flight (TOF) neutron powder diffractometer, NOVA at J-PARC. The samples were installed in a vanadium cell of 5.8 mm diameter. The diffraction data from the 90-degree banks was used for the structure analysis. The structure parameters are refined by the Rietveld method using the Z-Rietveld program.[40]

First-principles calculations were performed using the projected-augmented planewave method (PAW) within parametrization of the exchange-correlation functional by generalized gradient approximation (GGA) and the Perdew–Burke–Ernzerhof (PBE) in QUANTUM ESPRESSO.[41–43] The convergence with respect to plane-wave kinetic cutoff and *k*-point grids were carefully checked. The cutoff energy of 80.0 Ry (ca. 1088 eV) was used for all calculations, whereas the *k*-point grids of 3 × 3 × 3, 3 × 6 × 3, 3 × 3 × 6, and 9 × 9 × 6 were used for *P*4/*nmm*, *Pnma*, $P\bar{6}2m$, and *P*63/*mmc* of SrHF, respectively. The enthalpies were calculated by fitting the total energies as a function of the volume with the third-order Birch–Murnaghan isothermal equation of state (EOS) (details in Supporting Information).

Photoluminescence (PL) spectra were measured by using two monochromators (SP-2300i and SP-300i, Acton Research Corporation), a PMT detector (R928, Hamamatsu Photonics), and a xenon lamp (R300-3 J, Eagle Engineering Aerospace). Polycrystalline SrHF: Eu^{2+} (1%) samples were synthesized under high pressure using SrH_2, SrF_2 and EuH_x ($2 < x < 3$; 99.9%, Kojundo). The starting materials were mixed in a stoichiometric ratio and synthesized under the pressure of 1 and 3 GPa as has done with SrHF. The temperature was raised to 900 °C in 10 minutes, held for 1 hour, and then cooled to room temperature in 5 minutes.

Conflicts of interest

There are no conflicts to declare.

Acknowledgements

This work was supported by CREST project (JPMJCR1421), Grants-in-Aid for Scientific Research on Innovative Areas “Mixed Anion” (No. JP16H06439; JP16H06440; and 17H05491), and JSPS Core-to-Core Program (A) Advanced Research Networks (JPJSCCA20200004). The synchrotron radiation experiments were performed at the BL02B2 and BL32B2 of SPring-8, with the approval of the Japan Synchrotron Radiation Research Institute (JASRI) (2018B1073). The neutron experiments were conducted at J-PARC (2019B0382).

References

1 H. Kageyama, K. Hayashi, K. Maeda, J. P. Attfield, Z. Hiroi, J. M. Rondinelli and K. R. Poeppelmeier, *Nat. Commun.*, 2018, **9**, 772.
2 T. Yamamoto, D. Zeng, T. Kawakami, V. Arcisauskaite, K. Yata, M. A. Patino, N. Izumo, J. E. McGrady, H. Kageyama and M. A. Hayward, *Nat. Commun.*, 2017, **8**, 1217.
3 J. Bang, S. Matsuishi, H. Hiraka, F. Fujisaki, T. Otomo, S. Maki, J. Yamaura, R. Kumai, Y. Murakami and H. Hosono, *J. Am. Chem. Soc.*, 2014, **136**, 7221–7224.
4 F. Denis Romero, A. Leach, J. S. Möller, F. Foronda, S. J. Blundell and M. A. Hayward, *Angew. Chem. Int. Ed.*, 2014, **53**, 7556–7559.
5 N. Masuda, Y. Kobayashi, O. Hernandez, T. Bataille, S. Paofai, H. Suzuki, C. Ritter, N. Ichijo, Y. Noda, K. Takegoshi, C. Tassel, T. Yamamoto and H. Kageyama, *J. Am. Chem. Soc.*, 2015, **137**, 15315–15321.
6 T. Yajima, F. Takeiri, K. Aidzu, H. Akamatsu, K. Fujita, W. Yoshimune, M. Ohkura, S. Lei, V. Gopalan, K. Tanaka, C. M. Brown, M. A. Green, T. Yamamoto, Y. Kobayashi and H. Kageyama, *Nat. Chem.*, 2015, **7**, 1017–1023.
7 Y. Kobayashi, Y. Tang, T. Kageyama, H. Yamashita, N. Masuda, S. Hosokawa and H. Kageyama, *J. Am. Chem. Soc.*, 2017, **139**, 18240–18246.
8 Y. Tang, Y. Kobayashi, C. Tassel, T. Yamamoto and H. Kageyama, *Adv. Energy Mater.*, 2018, **8**, 1800800.
9 H. Yamashita, T. Broux, Y. Kobayashi, F. Takeiri, H. Ubukata, T. Zhu, M. A. Hayward, K. Fujii, M. Yashima, K. Shitara, A.

Kuwabara, T. Murakami and H. Kageyama, *J. Am. Chem. Soc.*, 2018, **140**, 11170–11173.
10 H. Ubukata, T. Broux, F. Takeiri, K. Shitara, H. Yamashita, A. Kuwabara, G. Kobayashi and H. Kageyama, *Chem. Mater.*, 2019, **31**, 7360-7366.
11 T. Broux, H. Ubukata, C. J. Pickard, F. Takeiri, G. Kobayashi, S. Kawaguchi, M. Yonemura, Y. Goto, C. Tassel and H. Kageyama, *J. Am. Chem. Soc.*, 2019, **141**, 8717-8720.
12 Y. Sato-Sorensen, *J. Geophys. Res.*, 1983, **88**, 3543–3548.
13 H. Oda, O. L. Anderson, D. G. Isaak and I. Suzuki, *Phys. Chem. Miner.*, 1992, **19**, 96–105.
14 S. J. Duclos, Y. K. Vohra, A. L. Ruoff, S. Filipek and B. Baranowski, *Phys. Rev. B*, 1987, **36**, 7664–7667.
15 J.-F. Brice, A. Courtois and J. Aubry, *J. Solid State Chem.*, 1978, **24**, 381–387.
16 J. F. Brice, M. Perrin and R. Leveque, *J. Solid State Chem.*, 1979, **30**, 183–188.
17 J. B. Forsyth, C. C. Wilson and T. M. Sabine, *Acta Crystallogr. Sect. A: Found. Crystallogr*, 1989, **45**, 244–247.
18 G. A. Kourouklis and E. Anastassakis, *Phys. Rev. B*, 1986, **34**, 1233–1237.
19 J. S. Wang, C. L. Ma, D. Zhou, Y. S. Xu, M. Z. Zhang, W. Gao, H. Y. Zhu and Q. L. Cui, *J. Solid State Chem.*, 2012, **186**, 231–234.
20 L. Gerward, J. S. Olsen, S. Steenstrup, M. Malinowski, S. Åsbrink and A. Waskowska, *J. Appl. Crystallogr.*, 1992, **25**, 578–581.
21 S. M. Dorfman, F. Jiang, Z. Mao, A. Kubo, Y. Meng, V. B. Prakapenka and T. S. Duffy, *Phys. Rev. B*, 2010, **81**, 174121.
22 J. S. Tse, D. D. Klug, S. Desgreniers, J. S. Smith, R. Flacau, Z. Liu, J. Hu, N. Chen and D. T. Jiang, *Phys. Rev. B*, 2007, **75**, 134108.
23 J. S. Smith, S. Desgreniers, D. D. Klug and J. S. Tse, *Solid State Commun.*, 2009, **149**, 830–834.
24 J. S. Tse, Z. Song, Y. Yao, J. S. Smith, S. Desgreniers and D. D. Klug, *Solid State Commun.*, 2009, **149**, 1944–1946.
25 J. M. Leger, J. Haines, A. Atouf, O. Schulte and S. Hull, *Phys. Rev. B*, 1995, **52**, 13247–13256.
26 R. D. Shannon, *Acta Crystallogr., Sect. A*, 1976, **32**, 751–767.
27 M. Glätzle, M. Schauperl, C. Hejny, M. Tribus, K. R. Liedl and H. Huppertz, *Z. Anorg. Allg. Chem.*, 2016, **642**, 1134–1142.
28 M. T. Anderson, K. B. Greenwood, G. A. Taylor and K. R. Poeppelmeier, *Prog. Solid State Chem.*, 1993, **22**, 197–233.
29 N. Kunkel, A. Meijerink and H. Kohlmann, *Inorg. Chem.*, 2014, **53**, 4800–4802.
30 N. Kunkel, D. Rudolph, A. Meijerink, S. Rommel, R. Weihrich, H. Kohlmann and T. Schleid, *Z. Anorg. Allg. Chem.*, 2015, **641**, 1220–1224.
31 J. Ueda, S. Matsuishi, T. Tokunaga and S. Tanabe, *J. Mater. Chem. C*, 2018, **6**, 7541–7548.
32 C. Pflug, A. Franz and H. Kohlmann, *J. Solid State Chem.*, 2018, **258**, 391–396.
33 F. H. Su, W. Chen, K. Ding and G. H. Li, *J. Phys. Chem. A*, 2008, **112**, 4772–4777.
34 T. Kobayasi, S. Mroczkowski, J. F. Owen and L. H. Brixner, *J. Lumin.*, 1980, **21**, 247–257.
35 N. Kunkel, H. Kohlmann, A. Sayede and M. Springborg, *Inorg. Chem.*, 2011, **50**, 5873–5875.
36 D. B. Gatch, D. M. Boye, Y. R. Shen, M. Grinberg, Y. M. Yen and R. S. Meltzer, *Phys. Rev. B Condens. Matter Mater. Phys.*, 2006, **74**, 195117.
37 F. H. Su, W. Chen, K. Ding and G. H. Li, *J. Phys. Chem. A*, 2008, **112**, 4772–4777.
38 M.-H. Fang, J. L. Leaño and R.-S. Liu, *ACS Energy Lett.*, 2018, **3**, 2573–2586.
39 J. Rodríguez-Carvajal, *Physica B*, 1993, **192**, 55–69.
40 R. Oishi, M. Yonemura, Y. Nishimaki, S. Torii, A. Hoshikawa, T. Ishigaki, T. Morishima, K. Mori and T. Kamiyama, *Nucl. Instrum. Methods Phys. Res., Sect. A,* 2009, **600**, 94–96.
41 P. Giannozzi, S. Baroni, N. Bonini, M. Calandra, R. Car, C. Cavazzoni, D. Ceresoli, G. L. Chiarotti, M. Cococcioni, I. Dabo, A. Dal Corso, S. de Gironcoli, S. Fabris, G. Fratesi, R. Gebauer, U. Gerstmann, C. Gougoussis, A. Kokalj, M. Lazzeri, L. Martin-Samos, N. Marzari, F. Mauri, R. Mazzarello, S. Paolini, A. Pasquarello, L. Paulatto, C. Sbraccia, S. Scandolo, G. Sclauzero, A. P. Seitsonen, A. Smogunov, P. Umari and R. M. Wentzcovitch, *J. Phys.: Condens. Matter*, 2009, **21**, 395502.
42 P. E. Blöchl, *Phys. Rev. B: Condens. Matter Mater. Phys.*, 1994, **50**, 17953–17979.
43 J. P. Perdew, A. Ruzsinszky, G. I. Csonka, O. A. Vydrov, G. E. Scuseria, L. A. Constantin, X. Zhou and K. Burke, *Phys. Rev. Lett.*, 2008, **100**, 136406.